JOURNAL OF AIRCRAFT
Vol. 43, No. 1, January–February 2006

Active Multiple Winglets for Improved Unmanned-Aerial-Vehicle Performance

Andrew Shelton,* Agvinesh Tomar,* JVR Prasad,† Marilyn J. Smith,‡ and Narayanan Komerath†
Georgia Institute of Technology, Atlanta, Georgia 30332-0150

The addition of a winglet to a flight vehicle is known to enhance cruise performance. The addition of multiple, active winglets to an existing unmanned aerial vehicle (UAV) is studied to determine the potential of these devices to augment both cruise and maneuvering performance. Passive and active multiple winglets are shown to increase range and endurance, providing the potential for increased payload. Active multiple winglets are shown to be a viable replacement for ailerons and to provide gust alleviation for improved handling qualities and sensor performance. Two methods of predicting winglet performance enhancements are applied and compared to the U.S. Marine Corps Dragon Eye UAV configuration.

Nomenclature

a_z	=	normal acceleration
C	=	specific fuel consumption
C_{Di}	=	induced drag coefficient
C_L	=	lift coefficient
D	=	drag
E	=	endurance
e	=	efficiency factor
g	=	gust
K	=	induced drag constant
K_1, K_2	=	proportionality constant
L	=	lift
R	=	range
S	=	wing area
W	=	weight
Δ	=	propeller efficiency

I. Introduction

As the aerospace industry has matured, interest in biological-based concepts to improve flight has revived. Of particular interest has been the practically of winglets to improve a vehicle's cruise performance. Richard Whitcomb at NASA Langley Research Center is credited with some of the first modern applications of winglets to transport aircraft, though the original patent dates back to 1897. In the mid- to late 1970s, Whitcomb compared the impact of a simple wing extension and a single, passive winglet added to a conventional wing.[1] The winglet doubled the wing's lift-to-drag ratio (L/D), along with a 20% reduction in induced drag, with comparable structural loading. Whitcomb also investigated near-vertical single passive winglets on a KC-135 (Ref. 2). These tests showed that winglets could increase an aircraft's range by as much as 7% at cruise speeds. Current applications on a Boeing 737-400 of a blended single, passive winglet[3] reduces drag by 7%, though wind-tunnel tests had indicated only 2% drag reduction.

Studies by biologists on birds with significant soaring capabilities indicate that that the source of their prodigious endurance is the tip or pin feathers that adjust with changing flight conditions. With the advent of light composite materials that can withstand high structural loading, the potential of implementing these more complex winglet systems is becoming more of a reality, and several concepts have been proposed and evaluated. Ilan Kroo et al.[4] have studied numerous concepts that generate nonplanar wakes, including winglets, ring wings, and box wings. The "spiroid" wing-tip[5] concept is similar to that of winglets in that it reduces induced drag. Spillman has investigated single and multiple sets of devices known "wing-tip sails" on wing-tip fuel tanks to improve performance.[6] An extension of this concept called WING-GRID[7] has been tested. The WING-GRID concept is a passive set of multiple wing extensions at various angles of attack truncated with a spanwise rib at the tip. Several of these concepts,[8] including the spiroid, blended winglet, and WING-GRID were experimentally evaluated recently, and significant modifications on the wing and in the wake were noted. There are negative issues associated with some applications of winglets that must be considered, including reduced flutter speed in transonic flows,[9] winglet airloads as a result of effect of sideslip,[10] and potential stability issues.[11]

Recent experimental studies with a symmetric airfoil wing[12] have shown that wings with fixed multiple winglets can attain a 15 to 30% lift-to-drag characteristic rather than wings with single winglets in the low-Reynolds-number regime characteristic of unmanned aerial vehicles (UAVs). This increased efficiency over a plain wing or single winglet performance is achieved by splitting the single tip vortex into lower strength multiple vortices by controlling the individual winglet angles of attack, dihedral, and sweep as flight conditions and/or mission requirements change. Active control of the winglets further optimizes the wing for specific flight conditions, resulting in improved performance parameters such as endurance and range. Actively controlled multiple winglets also have the potential to perform the function of ailerons and other control surfaces. Santos[13] originally patented the idea of multiple winglets rather than one winglet at the wing tip, but permitted his patent to expire.

This paper extends the active multiple winglets concept to an existing unmanned aerial vehicle, the U.S. Marine Corps Dragon Eye, and demonstrates the resulting improved performance and maneuvering characteristics. Results presented in this paper consist of performance data from an aerodynamic panel code and from an active control simulation. The code PMARC-12 is used to optimize the winglet configuration for the planform and different flight conditions. This panel method has been validated against numerous configurations as well as recent winglet wind-tunnel results. The active control simulation is utilized to also evaluate performance and to explore maneuvering flight. The active controller development is based on an adaptive neural net controller architecture. This controller architecture was developed at the Georgia Institute of

Presented as Paper 2004-4968 at the 22nd Applied Aerodynamics Conference and Exhibit, Providence, RI, 16–19 August 2004; received 15 October 2004; revision received 19 January 2005; accepted for publication 27 January 2005.

*Graduate Research Assistant, School of Aerospace Engineering. Student Member AIAA.
†Professor, School of Aerospace Engineering. Associate Fellow AIAA.
‡Associate Professor, School of Aerospace Engineering. Associate Fellow AIAA.

Technology under the Center of Excellence in Rotary Wing Technology and was successfully flight tested on the X-36 fixed-wing UAV and the R-50 Helicopter UAV.

II. Methodology

A. PMARC-12 Aerodynamic Simulation

To perform the optimization and performance studies efficiently, a lower-order aerodynamic method, PMARC-12, was deemed to be more appropriate than more complex higher-order computational-fluid-dynamics (CFD) methods. Although PMARC-12 uses a lower-order panel method based on constant doublet and vortex strengths, such methods have been shown to provide excellent correlation with experimental data for simple geometries such as the wings and winglets studied here. The time-stepping wake model assumes that the wake convects downstream from the wake-separation line by the local velocity. At each time step, a new row of wake panels is added to the wake using the local velocity as the guide for the position of the panels. The option is also given to prescribe the wake, as in steady flow cases where the wake is assumed to move downstream along a constant plane. Problems are encountered with PMARC when the wake encounters another wake panel (as shed from another winglet) or when the wake panel makes contact with a solid surface (such as a following winglet). To circumvent these problems for steady flows, the wake can be prescribed near the winglets to ensure that the code starts properly, and then a free wake can continue past a certain reference time when the wake has traveled beyond the winglets. An additional option exists to continue the computation even though there has been an interaction.

B. Active Control Simulation

Several active control schemes have been formulated for these evaluations based on 1) effectiveness of the scheme for mode alleviation, wing aerodynamic performance improvement, and ride quality improvement (i.e., disturbance rejection capability); 2) viability of the scheme in terms of hardware implementation, and 3) overall impact in terms of cost and weight.

The formulation of the schemes makes use of two competing philosophies:

1) The first is active control of winglets for enhancement of aerodynamic performance and for suppression of undesirable aerodynamic effects. Using appropriate flow sensors (for example, dynamic pressure sensors), the dynamic flow environment on the wing will be measured and will be used for active control of winglet orientation to achieve enhanced aerodynamic performance of the wing.

2) Active control of winglets for mode alleviation is the second philosophy. Using appropriate sensors (for example, strain gauge sensors) at preselected locations on the wing, the structural response of the wing to atmospheric disturbances will be measured and used for active control of winglet orientation to achieve reduced vibration and enhanced ride quality.

III. Correlation of the Panel Method

Panel optimization studies were performed to ensure that the best representation of the main wing and the winglets is obtained in the numerical simulations. A parametric study showed that the most efficient number of panels (per surface) is 45 in the chordwise direction and 10 in the spanwise direction. These panel values yielded less than 1% difference in lift, induced drag, and moment ($c/4$) coefficients than finer grids. Induced drag showed minor differences when integrated or when using a Treffz plane.

A symmetric wing configuration, which was experimentally evaluated,was utilized to correlate the results in conjunction with data from Abbott and von Doenhoff.[14] The actual model coordinates measured at a random location were utilized to provide error analysis with respect to the original wing airfoil. The airfoil model (Fig. 1) was compared with baseline NACA0015 and NACA0016 airfoil shapes obtained from Abbott and von Doenhoff.[14] The upper surface of the model wing approximated very closely the NACA0015 airfoil. On the lower surface, the airfoil matched the NACA0016 airfoil more closely near the leading edge than it does the NACA0015

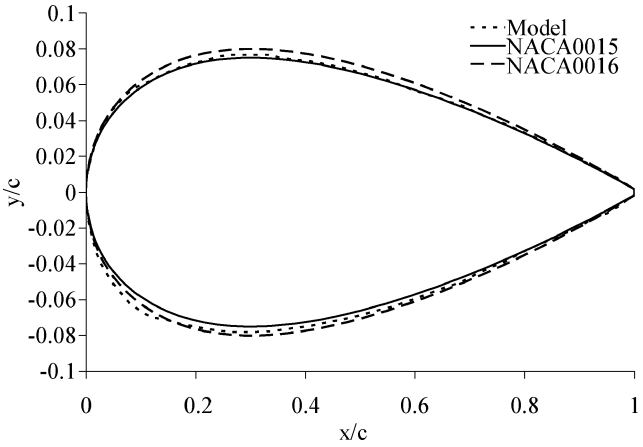

Fig. 1 Comparison of model airfoil with NACA0015 and NACA0016 airfoils.

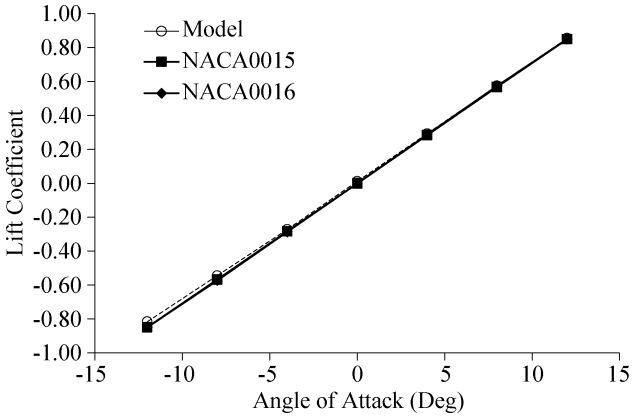

Fig. 2 Comparison of wing lift coefficients using PMARC.

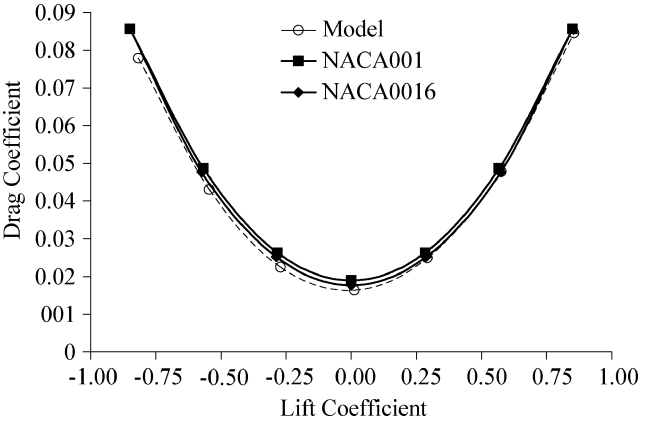

Fig. 3 Comparison of wing inviscid drag coefficients using PMARC.

airfoil. This uneven representation of surfaces resulted in a slight negative camber near the leading edge of the wing.

The PMARC code has an built-in option for NACA four-digit series airfoils. However, these airfoils are artificially closed at the trailing edge by the program, which affects calculations of the aerodynamic coefficients. Therefore, in order to effect more commonality in the comparison of the model airfoil with the NACA0015 and NACA0016 airfoils, the airfoil coordinates for the latter two were generated by the NACA four-digit series equations provided by Abbott and von Doenhoff.[14] These sections have open trailing edges, similar to the model. The results of these predictions are provided in Figs. 2–4. Analysis of the lift-curve slopes show very little difference, as expected from the closeness of the airfoil shapes. Comparison with two-dimensional experimental data of Abbott and von

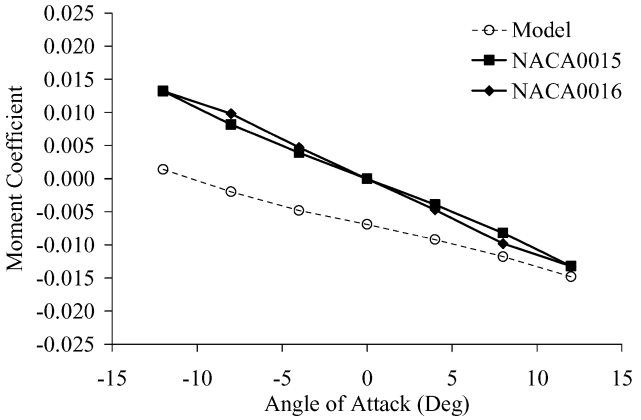

Fig. 4 Comparison of wing quarter-chord moment coefficients using PMARC.

Doenhoff,[14] corrected for aspect ratio, shows that PMARC lift-curve slopes are within 5% of the anticipated values. (Two-dimensional corrected value is 0.084; PMARC NACA values are 0.0868 and 0.088; PMARC model value is 0.0865.) The effect of the model camber is to shift the zero-lift angle of attack from 0 to −0.15 deg, as shown by the PMARC data. The experimental data show that the lift-curve slope of the baseline winglet configuration has shifted even farther, indicating that the wing model airfoil might not be uniform across the span.

The drag data show the correct trend anticipated from drag polars. There is an upward shift from the two-dimensional values, as expected from the impact of the finite wing. Evaluation of the induced drag effects was made using the standard equation

$$C_{\mathrm{Di}} = C_L^2 \big/ \pi e \mathrm{AR} \tag{1}$$

where aspect ratio (AR) = 8, and e is approximately 0.89 for a uniform wing of this aspect ratio. Comparison with the PMARC data showed approximately 10 to 11% difference. Overall drag includes the blunt trailing-edge effects. Moment data appear to be similar to the experimental results, given the very poor resolution of the scales in Abbott and von Doenhoff.

The winglet configuration was optimized within the baseline PMARC code. In the experiment, the winglets are flat plates rather than classic aerodynamic airfoil shapes. Efforts were undertaken to model the winglets as flat plates so that the numerical model more exactly matches the experimental model. However, PMARC-12 has a problem modeling flat plates in an aerodynamic flow. Starting with an ellipse that accurately modeled the winglet thickness, the leading- and trailing-edge radii were reduced in steps in an attempt model the machined winglets as closely as possible. The winglets were also mounted as closely as possible to the experimental configuration, although the actual mounts were neglected. Finally, a parametric study similar to that for the baseline wing was undertaken to ensure that the most accurate, yet efficient grid was utilized for the remainder of the simulations.

Comparisons of the lift coefficient for the baseline wing and the wing with winglets at 0 deg are shown in Fig. 5. The lift is slightly increased, and comparably the drag is slightly decreased. There exist some difficulties at low angles of attack for the PMARC code with the winglets at zero-deg incidence with respect to the wing. This is because of the interference of the wakes emanating from the winglets.

Similar to the experimental results, the numerical results show that the addition of the winglets improves the lift-curve slope by the addition and manipulation of the winglets, as seen in Table 1. The best results were obtained when the winglets were spaced at equal dihedral angles of 10 deg, with the most forward winglet deflected by 20 deg. The correlation of the PMARC with the experimental results was larger than expected; the two-dimensional comparisons already discussed showed much closer correlation. It was known during the tests that the balance sensitivity at lower speeds, as well as some

Table 1 Lift-curve slopes (per radian) for untripped wing

Source	Base wing	Winglets at 0 deg	20, 10, 0, −10, and −20 deg
Exp −25 ft/s	3.99	4.07	4.89
Exp −65 ft/s	4.25	4.31	4.96
Exp −85 ft/s	N/A	4.62	N/A
Panel code	4.99	5.09	5.33

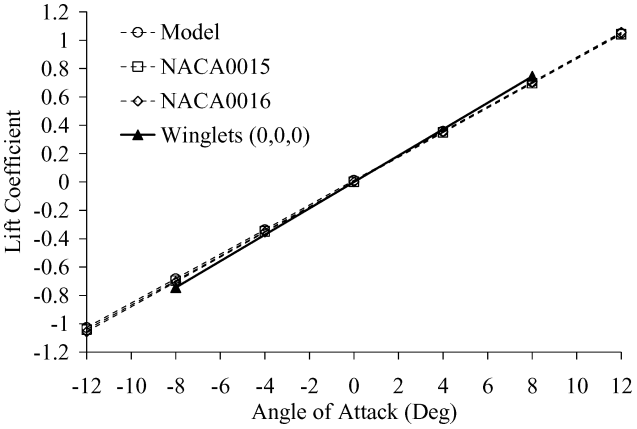

Fig. 5 Effect of multiple fixed winglets on baseline wing.

observed deflections of the model during the experiments, might be an issue. Further, comparison of other experimental results at low Reynolds numbers (less than 3×10^5) also show wide experimental scatter. For example, the computed three-dimensional lift-curve slope for the NACA0009 from two-dimensional experiments[15,16] varies from 4.25 to 5.05. Comparisons were made with a rectangular wing of aspect ratio 8 using the NACA0012 airfoil, which has been tested in the same tunnel at Georgia Tech.[12] Using a CFD code, COBALT,[17] the NACA0012 airfoil was run using various viscous modeling options and corrected to the three-dimensional test configuration. The hypothesis of the experiment discrepancy is further confirmed when these results are compared; the Selig lift-curve slope[15] is 4.45, the GIT experimental value is 5.33, and the Cobalt results all fall at about 4.6. These variations indicate that the scatter in the experiment and computations remain large at these low Reynolds numbers, justifying the use of PMARC results, which show consistent, conservative trends for the baseline and winglet configurations with the experimental data.

During the experimental portion of this project, a laser sheet was used to illuminate cross sections of the flow downstream of the wing tip trailing edge, with smoke patterns videotaped from downstream. Comparable streamlines were plotted using the results of the panel code for visual correlation with the experimental data. As seen in Fig. 6, the panel method shows the streamlines rolling up into the tip vortex for the baseline wing at an angle of attack of 5 deg. In Fig. 7, the winglets were added to the configuration, and two vortices form—one at the main baseline wing tip and another from the collective winglets set at the same dihedral of 0 deg. Figure 8 shows experimental flow visualization from Ref. 1, which indicates that the five-winglet vortices of the optimal 10-deg dihedral spacing are distinct. Similar results can be seen from the simulations in Fig. 9. Coalescence of the winglet vortices does not occur until 8 to 10 chords downstream of the wing.

IV. Results

A. Dragon Eye Configuration

Comparisons were next made with the Dragon Eye UAV. Basic characteristics of the configuration can be viewed in Table 2. A three view of the Dragon Eye that illustrates the full configuration with the winglets added is shown in Fig. 10.

Table 2 Basic characteristics of the Dragon Eye UAV[a]

Parameter	Characteristic
Wing span	45 in. (1.14 m)
Length	35.75 in. (0.91 m)
Weight	5 1b (2.28 kg)
Cruising speed	60 ft/s (18 m/s)
Altitude	300 to 500 ft AGL (91 to 122 m AGL)[b]
Flight time	30 to 60 min

[a]Data available online at http://www.globalsecurity.org/intell/systems/dragon-eye.htm.
[b]AGL = above ground level.

Fig. 6 Streamlines from PMARC-12 for the baseline wing.

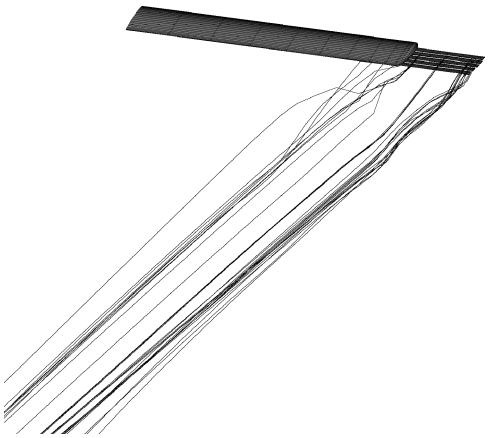

Fig. 7 Streamlines from PMARC-12 for the baseline wing with winglets at zero dihedral.

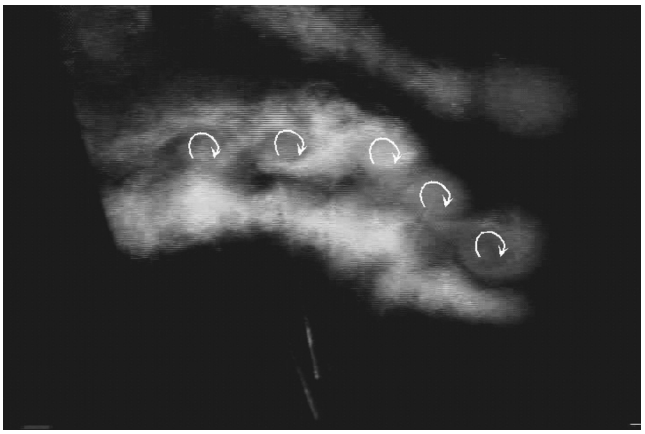

Fig. 8 Winglets at +20, +10, 0, −10, and −20 deg dihedral. Laser plane at two chords downstream of trailing edge; angle of attack 6 deg.

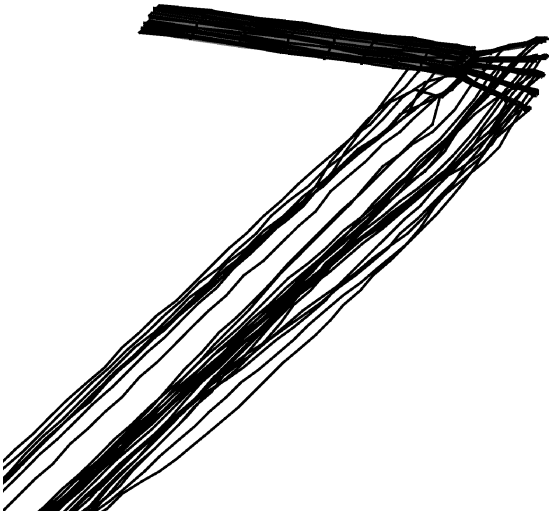

Fig. 9 Streamlines of a panel code for the baseline wing with winglets at +20, +10, 0, −10, and 20 deg.

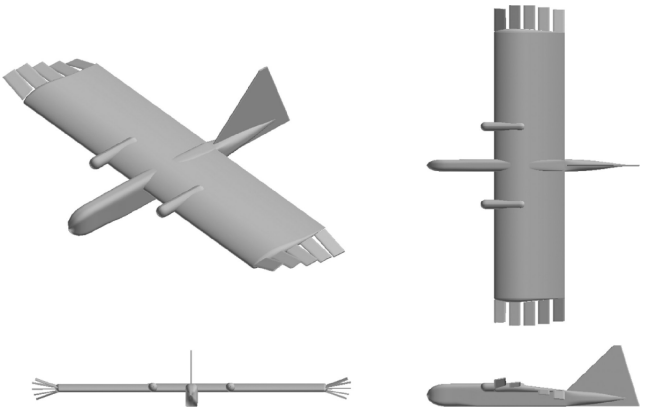

Fig. 10 Three view of Dragon Eye configuration with winglets.

B. Winglet Cruise Performance Evaluation

Two method—a PMARC-12 aerodynamic panel method simulation and a neural-network-based analysis—were utilized to evaluate the cruise performance of the vehicle with and without the winglets. For the panel method study, a composite body for the Dragon Eye was extrapolated from CAD drawings and into GRIDGEN to develop a smoothly varying body. This last step was accomplished so that the wing/body, body/tail, and wing/nacelle interfaces could be properly smoothed to prevent nonphysical results from the aerodynamic simulation. Using PMARC-12, the Dragon Eye configuration was studied for a series of winglet span sizes [4 in. (10.16 cm), 8 in. (20.32 cm), and 12 in. (30.48 cm)] and various dihedral and angle-of-attack combinations. As was also determined in prior applications on a baseline NACA0015 wing, the optimal five-winglet dihedral spread was found to be in 10-deg increments, beginning with +20 deg and ending with −20 deg. Additionally, the optimal five-winglet angle-of-attack incidences were confirmed to be −10, −6, 0, 2, and 5 deg.

In Figs. 11–14, the evaluation of a wing with different winglet spans is shown compared with the baseline wing. The increase in lift-curve slope varies nearly linearly with span increase. However, the parasite drag associated with the larger surface area of the winglets takes a progressively higher lift before it has a positive benefit on the overall drag of the system. The quarter-chord pitching moment is increasingly negative with the winglet span addition, and the moment-lift slope also changes direction compared with the baseline.

For the Dragon Eye configuration, the lift coefficient for cruise flight requires a lift coefficient of 0.34. As shown in Figs. 11–14, this corresponds to the location at which winglets begin to have a pronounced improvement on the L/D with respect to the baseline configuration. Additionally, Fig. 14 shows that a comparable L/D

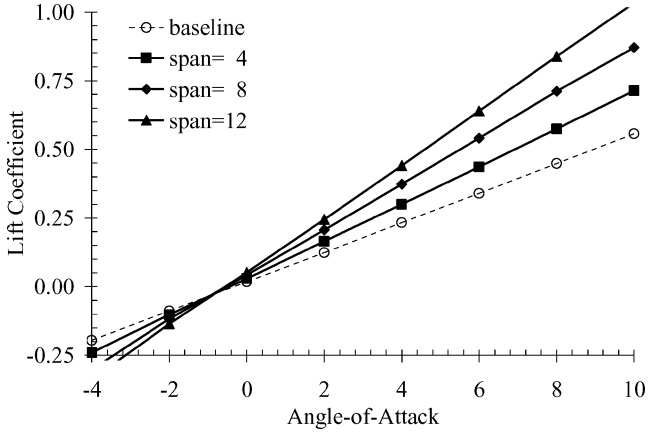

Fig. 11 Dragon Eye winglet span study: lift.

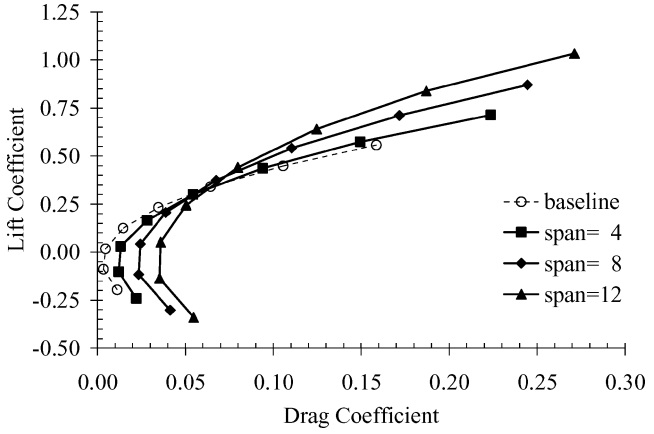

Fig. 12 Dragon Eye winglet span study: drag.

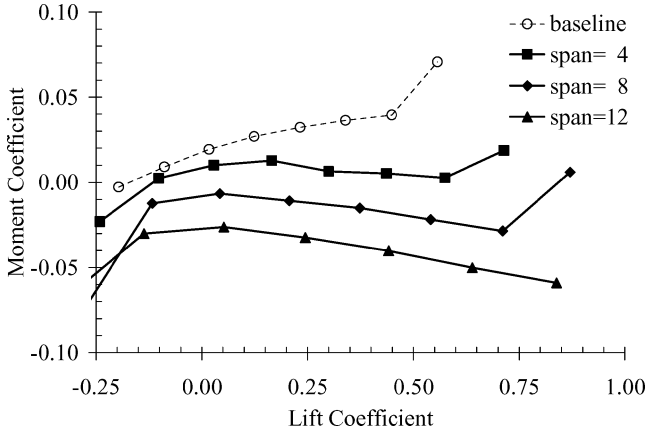

Fig. 13 Dragon Eye winglet span study: moment.

can be maintained by the 8- (20.32-) and 12-in. (30.48-cm) winglets for higher lift coefficients. This indicates that the payload can be increased by approximately 30% without a penalty in most performance categories, providing the option to add sensors or increase the size of the battery for greater power or endurance.

For the neural-network simulations, the Dragon Eye flight data from the Navy (primarily the flight envelope, lift and drag coefficients, longitudinal and lateral stability derivatives and control sensitivities) were used to modify the simulation model previously developed for a transport aircraft. Experimental data for the five winglet configuration consisted of lift and drag coefficients at different angles of attack of the wing and different angles of attack of first winglet. These data were used to develop functional relationships with the angles of attack of the wing and the first winglet as

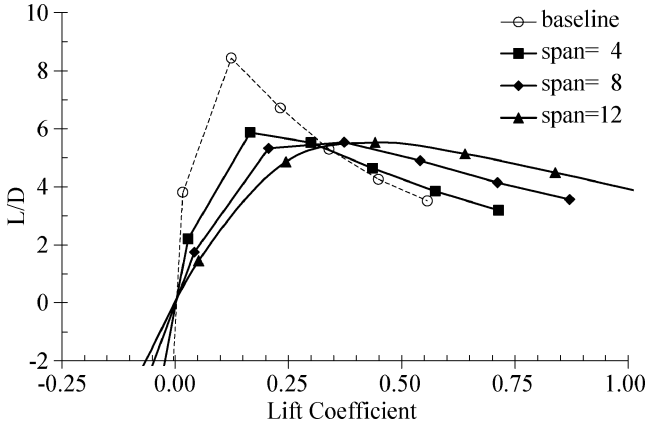

Fig. 14 Dragon Eye winglet span study: lift/drag.

inputs and the corresponding changes in lift and drag coefficients as outputs. Because the angles of attack of other four winglets and dihedral angles of all five winglets were fixed in experiments, they could not be used as independent variables in developing these functions. It was assumed in these calculations that the wing span was reduced by the length of the added winglets so that both the baseline wing and wing with winglets had an equivalent span. Further, because the winglets were evaluated for control purposes, it is assumed that the mechanisms for roll control were removed from the wing and replaced by the winglet sensors and control, so that the UAV maintained an essentially constant weight for the comparison. Analysis of this UAV indicated that the loading on the wing and winglets would not substantially change because of the low flight speed. Application of winglets to other configurations should include an evaluation of the structural loads and moments generated by the winglets and their impact on the wing itself. Complications such as those discussed in the Introduction, such as flutter, might be encountered and cannot be ignored.

To analyze the improvement in aerodynamic cruise performance with winglets, the simulation model was used to calculate L/D at different trim speeds in a straight and level flight. At each trim speed, the angle of attack of the first winglet was set to a value that would maximize L/D at that speed. The first winglet angle of attack was the only variable that could be changed to maximize L/D because all other winglets were fixed and no experimental data were available corresponding to their variation for the Georgia Tech configuration. Figure 15 compares C_L vs C_D variation for the Dragon Eye with and without winglets. Note that in the presence of winglets C_D decreases for a given value of C_L, indicating an increase in L/D. Also, note that the maximum C_L obtained is about 1.25 because of stall characteristic [min. trim speed = 35 ft/s (10.7 m/s)] and minimum C_L is about 0.2 because of maximum power limitation [max speed = 80 ft/s (24.4 m/s)]. From Fig. 15 it is clear that with a decrease in speed C_L increases as does the induced drag. The winglets increase the effective wing span, which in turn reduce the induced drag constant K, where

$$C_D = C_{D0} + KC_L^2 \tag{2}$$

Given that ΔK is the change in induced drag constant, change in drag coefficient is given by

$$\Delta C_D = \Delta K C_L^2 \tag{3}$$

which is proportional to C_L^2. This figure correlates very closely with the aerodynamic results of the PMARC-12 analysis that was obtained using the CAD configuration (Fig. 10). Thus, the aerodynamic performance gains can be comparably estimated by either method. Further, the flat-plate winglet results on the NACA 0015 experimental wing correlate well when analyzed with the baseline Dragon Eye characteristics.

Figure 16 compares the lift-to-drag ratio at different trim speeds with and without winglets. Note that the lift-to-drag ratio increases considerably at low speeds when winglets are added. However, at

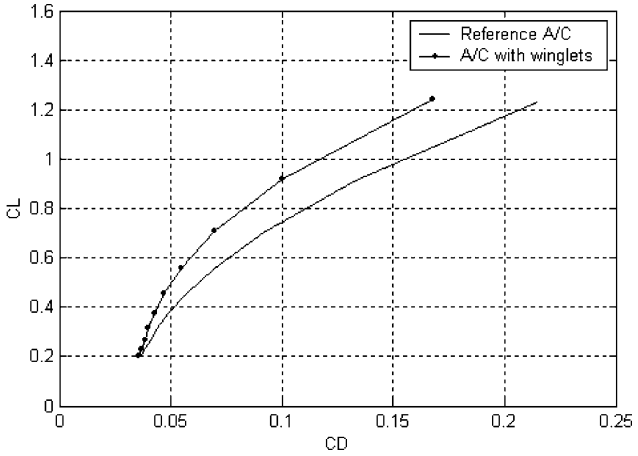

Fig. 15 Comparison of lift and drag coefficients, with and without winglets.

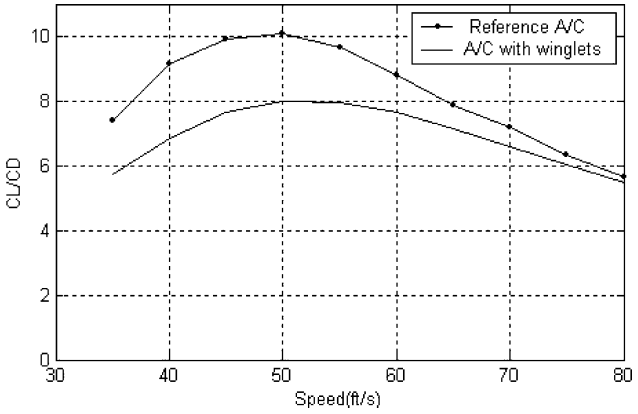

Fig. 16 Lift-to-drag ratio vs speed, with and without winglets.

larger speeds the increase is not so significant. Also from Fig. 16 the maximum lift-to-drag ratio is about 8.0 without winglets and 10.0 with winglets, and the corresponding trim speed is about 50 ft/s (15.2 m/s).

Figure 17 shows the percent increase in range when winglets are employed. Assuming that range is proportional to L/D, we can get an estimate of the increase in range through the increase in L/D at different speeds using Fig. 17. For a propeller-driven aircraft, range can be obtained using the following equation:

$$R = K_1(\eta/c)(L/D)(1/W) \tag{4}$$

Thus change in endurance is proportional to change in L/D. The percentage increase in the range is larger at lower speeds because of high C_L required (at high C_L winglets are more effective), but that does not mean that lowest speed will correspond to maximum range. The percent increase in maximum range is about 26%, which corresponds to a speed of 50 ft/s (15.2 m/s). Similarly, increase in endurance can be estimated when winglets are employed. Figure 18 shows the percentage change in endurance with winglets for the Dragon Eye. For a propeller-driven aircraft, endurance can be obtained using the following equation:

$$E = K_2(\eta/c)\left(C_L^{1.5}/C_D\right)\sqrt{S/W} \tag{5}$$

Thus change in endurance is proportional to change in $C_L^{1.5}/C_D$.

The impact of the size of the winglets on range and endurance is provided in Table 3, where an increased lift coefficient of 0.45 is selected to illustrate the improvement gains of the winglets. The addition of 4-in. (10.16-cm) winglets to the baseline wing yields a modest 5% increase in range or endurance. However, additional 4-in. (10.16-cm) increases in the winglet span [from 4 in. (10.16 cm) to 8 in. (20.32 cm) and from 8 in. (20.32 cm) to 12 in. (30.48 cm)] yield incremental improvements of 15 and 10%.

Table 3 Improvement in range and endurance for the Dragon Eye UAV with winglets

Winglet span, in. (cm)	Change in range or endurance,[a] %
4 (10.16)	5
8 (20.32)	20
12 (30.48)	30

[a]A lift coefficient of 0.45 is utilized.

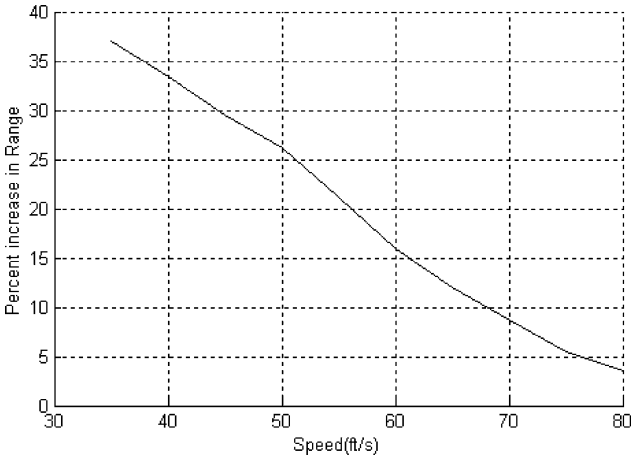

Fig. 17 Percent increase in range as a function of speed when winglets are employed.

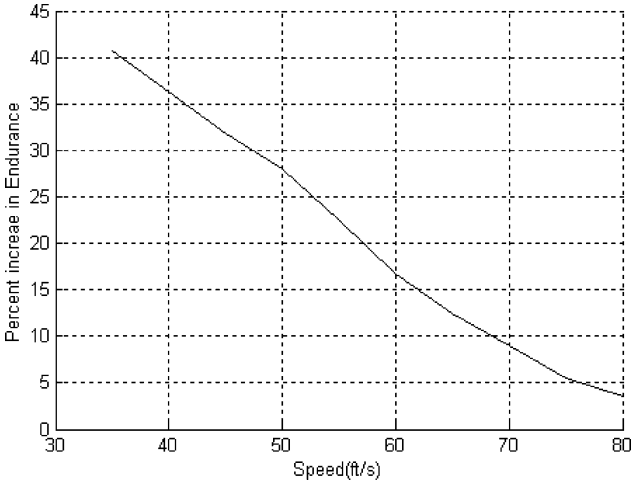

Fig. 18 Percent increase in endurance as a function of speed when winglets are employed.

C. Maneuvering Simulations

In addition to reducing the induced drag, a differential orientation change of the winglets can be used in place of ailerons for generating a rolling moment and controlling roll dynamics. Because of the large arm length from the center of gravity, winglets can create considerable rolling moment. This aspect was explored by obtaining the control surface deflection required for trimming the aircraft in a level flight at different sideslip angles. The dotted line shown in Fig. 19 is the aileron deflection required for trimming at different sideslip conditions without winglet control. The solid line shows winglet deflection required for trimming without the aileron control. Winglet control surface deflection is defined as the change in angle of attack of first winglet, positive on one side and negative on other side of the wing, from a trim value of -10 deg. Note that for the particular winglet geometry used in this study, winglet deflection is larger relative to that required for aileron deflection. At high sideslip angles the winglet deflection required no longer varies linearly, because of the nonlinear relation of lift generated with the winglet angle of attack.

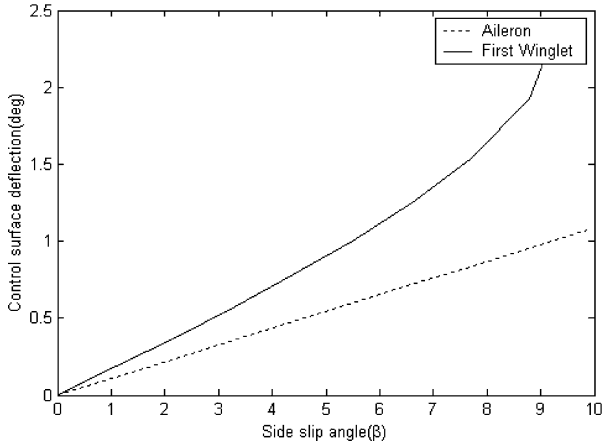

Fig. 19 Control deflection required in steady sideslip.

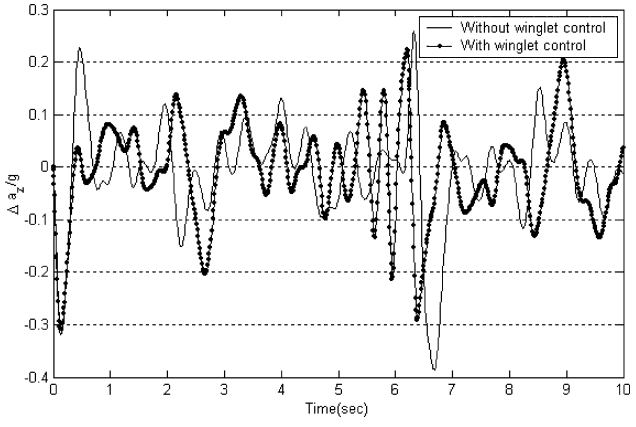

Fig. 20 Response to a random gust.

The gust response alleviation characteristics of winglets were analyzed by subjecting the Dragon Eye configuration to a random vertical gust of 5-ft/s (1.5 m/s) intensity with and without active winglet control. The gust profile was generated using the Dryden gust model. The trim speed was taken to be 60 ft/s (18.3 m/s) at an altitude of 2000 ft (610 m), and the first winglet angle of attack was used as the control. A saturation limit from -15 to -5 deg was assumed for the control (first winglet angle of attack) because of the range of available experimental data. Because the gust profile is random, the rms value of normal acceleration response to gust $\Delta a_z/g$ is considered as the measure of response. The simulation model was run a few times, with and without active winglet control, and the rms values of normal acceleration response were obtained. On an average the use of winglet control resulted in roughly 13% reduction in the rms response to random gust. Figure 20 shows two typical gust response profiles, one with active winglet control and another without active control.

V. Conclusions

The addition of multiple, actively controlled winglets can be utilized to modify the performance of vehicles in low-speed flight—in particular UAVs. This performance modification can be utilized to enhance the performance and/or maneuverability of these vehicles at different times during their mission.

Two types of analysis that utilize different data were evaluated. The first method employed a panel method using a CAD geometry to affect parametric studies of the configuration. The second method utilized known characteristics of the baseline model and winglet results from a generic wing. Although the results of the two analyses were not the same (as anticipated), the predicted trends were strikingly similar.

For steady performance analysis, it is shown that a wing with multiple winglets,compared with a baseline wing of the same aspect ratio, will result in an up to 40% increase in range and endurance. In addition, the winglets generate a shift of the maximum lift-to-drag ratio with respect to the cruise lift coefficient to a higher lift coefficient, indicating the ability of the winglets to increase the payload of the vehicle. These increases were seen with both passive and active multiple winglets. Analysis has shown that these winglets can also be utilized to replace control surfaces and indicate the potential applicability of active winglets for ride enhancement by negating the effects of gust impingement on the vehicle.

Acknowledgments

This work was funded as part of a subcontract to an Air Force Research Lab Small Business Research Phase 1 and 2 project, under Contract Nos. F33615-00-C-3017 and F33615-01-C-3120, respectively, entitled “Multi-Winglets for Reduction of Induced Drag.” Star Technology and Research, Inc., was the prime contractor on this effort. The authors would like to thank Jerome Pearson of Star Technology and Research, Inc., for his support and background efforts upon which this research was based. The authors would also like to thank Chuck Jobe and Dennis Carter, the U.S. Air Force technical monitors, for their technical insights during the project.

References

[1]Whitcomb, R., “A Design Approach and Selected Wind-Tunnel Results at High Subsonic Speeds for Wing-Tip Mounted Winglets,” NASA TN D-8260, July 1976.

[2]Whitcomb, R., “Methods for Reducing Aerodynamic Drag,” NASA CP 2211, *Proceedings of Dryden Symposium*, Sept. 1981.

[3]French, R. V., “Vortex Reducing Wing Tip,” U.S. Patent 4,108,403, 22 Aug. 1978.

[4]Kroo, I., McMasters, J., and Smith, S. C., “Highly Nonplanar Lifting Systems,” *Proceedings of the Transportation Beyond 2000: Technologies Needed for Engineering Design*, NASA Langley Research Center, Sept. 1995.

[5]Gratzer, L. B., “Spiroid-Tipped Wing,” U.S. Patent 5,102,068, 7 April 1992.

[6]Spillman, J. J., “The Use of Wing Tip Sails to Reduce Vortex Drag,” *Aeronautical Journal*, Vol. 82, No. 813, Sept. 1978, pp. 387–395.

[7]La Roche, U., and Palffy, S., “WING-GRID, a Novel Device for Reduction of Induced Drag on Wings,” *Proceedings of ICAS 96*, Sorrento, 1996.

[8]Soltani, M. R., Ghorbanian, K., and Nazarinia, M., “Flow Analysis Over and Behind a Wing with Different Winglet Shapes,” *42nd AIAA Aerospace Sciences Meeting and Exhibit*, AIAA, Reston, VA, 2004, pp. 8329–8338; also AIAA Paper 2004-723, 2004.

[9]Ruhlin, C. L., Bhatia, K. G., and Nagaraja, K. S., “Effects of Winglet on Transonic Flutter Characteristics of a Cantilevered Twin-Engine Transport Wing Model,” NASA TP 2627, Dec. 1986.

[10]Meyer, R. R., Jr., and Covel, P. F., “Effects of Winglets on a First-Generation Jet Transport Wing: VII—Sideslip Effects on Winglet Loads and Selected Wing Loads at Subsonic Speeds for a Full-Span Model,” NASA TP 2619, Sept. 1986.

[11]Satran, D. R., “Wind-Tunnel Investigation of the Flight Characteristics of a Canard General-Aviation Airplane Configuration,” NASA TP 2623, Oct. 1986.

[12]Smith, M. J., Komerath, N., Ames, R., Wong, O., and Pearson, J., “Performance Analysis of a Wing with Multiple Winglets,” AIAA Paper 2001-2407, June 2001.

[13]Santos, J., “Wingtip Airfoils,” U.S. Patent 4,595,160, 17 June 1986.

[14]Abbott, I., and von Doenhoff, A., *Theory of Wing Sections*, Dover, New York, 1949.

[15]Selig, M., Donovan, J., and Fraser, D., “Airfoils at Low Speed,” SoarTech #8, SoarTech, Virginia Beach, VA, 1989.

[16]Jacobs, E. N., and Sherman, A., “Airfoil Section Characteristics as Affected by Variations of the Reynolds Number,” NACA Rept. 586, 1937.

[17]Strang, W. Z., Tomaro, R. F., and Grismer, M. J., “The Defining Methods of Cobalt60: a Parallel, Implicit, Unstructured Euler/Navier–Stokes Flow Solver,” AIAA Paper 99-0786, 1999.